Manuscript prepared for Biogeosciences
with version 2015/04/24 7.83 Copernicus papers of the LaTeX class copernicus.cls.
Date: 3 June 2016

Methods to Retrieve the Complex Refractive Index of Aquatic Suspended Particles: going beyond simple shapes

A.-M. Sánchez[1] and J. Piera[1]

[1]Institute of Marine Sciences (ICM-CSIC), Physical and Technological Oceanography Department, Pg. Marítim de la Barceloneta, 37-49, 08003, Barcelona, Spain

Correspondence to: A.-M. Sánchez (amsanchez@icm.csic.es)

Abstract. The scattering properties of aquatic suspended particles have many practical applications in aquatic optics. In particular, several methods have been proposed to estimate important features of the particles by inversion from optical measurements, such as their size distribution or their refractive index. Most of the proposed methods are based on the Lorenz-Mie theory to solve Maxwell's equations, in which particles are considered homogeneous spheres. A generalization that allows considering more complex shaped particles is the T-matrix method. Although this approach imposes some geometrical restrictions -particles must be rotationally symmetric-, it is applicable to many life forms of phytoplankton. In this paper, the performance of several inversion methods for the retrieval of the refractive indices are compared considering three different synthetic scenarios. The error associated with each method is discussed and analyzed. The obtained results suggest that inverse methods using the T-matrix approach are useful to retrieve the refractive indices of complex shapes (i.e., many phytoplankton species) accurately.

1 Introduction

Light interactions with aquatic particles are the processes by which changes of the composition of small particles suspended in the water column (such as phytoplankton, sediment or microplastics), cause optical observable phenomena that usually are wavelength dependent (for example, changes on the ocean color or the light extinction with depth) (Mobley, 1994; Kirk, 1994). Understanding the interaction of light with particles is the central topic in many bio-optical studies in which the water particle composition is inferred from $in\text{-}situ$ or remote sensing optical observations (Gordon and Morel, 2012, and references therein).

Maxwell's equations are the basis of theoretical and computational methods describing light interaction with particles. However, exact solutions to Maxwell's equations are only known for selected geometries. Scattering from any homogeneous spherical particle with arbitrary size parameter is explained analytically by the Lorenz–Mie (also known as Mie) theory (Lorenz, 1898; Mie, 1908).

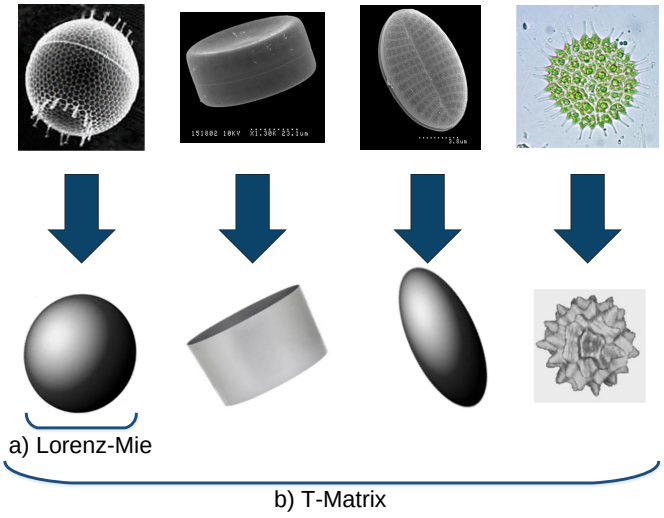

Figure 1. Lorenz-Mie (a) only describes the scattering of an electromagnetic plane wave by a homogeneous sphere, while T-Matrix (b) also characterizes the scattering by non-spherical particles such as spheroids, cylinders or Chebyshev particles. As shown by Clavano et al. (2007), aspect ratios of phytoplankton (ratio of the principal axes of a particle) span between 0.4 and 72.

Although most of the bio-optical models assume that particles are spheres, it is generally accepted that most of the particles that contribute significantly to light interactions are non-spherical (Clavano et al., 2007, and references therein). For more complex shaped particles, scattering can be computed using the T-Matrix theory (Waterman, 1965). At present, the T-Matrix method is the fastest exact technique for the computation of nonspherical scattering based on a direct solution of Maxwell's equations (Mischenko et al., 1996). Although there are some geometrical restrictions, such as axial symmetry, it is applicable to many life forms of phytoplankton and suspended mineral particles (Quirantes and Bernard, 2004; Sun et al., 2016), as shown in Fig. 1.

Both approximations to solve Maxwell's equations share one important requirement: the complex refractive index of the particles must be known. Although new promising techniques such as Tomographic Phase Microscopy (Choi et al., 2007) may provide in the future measurements of the refractive index in live cells, at present current ocean instrumentation do not directly provide it, so it must be estimated somehow (Aas, 1996).

Several inverse models to retrieve the refractive index from optical measurements can be found in the literature. For instance, a single equation based on the Lorenz-Mie theory is used by Twardowski et al. (2001), to estimate the refractive index of a bulk oceanic distribution. It is indeed a fast method if optical backscattering measurements are available. Stramski et al. (1988) presented an extension of a model from Bricaud and Morel (1986), designed for isolated phytoplankton cultures (or dominance of one particular phytoplankton species). It is based on the anomalous diffraction approximation (ADA), which allows the computation of the real and imaginary parts of the complex refractive index

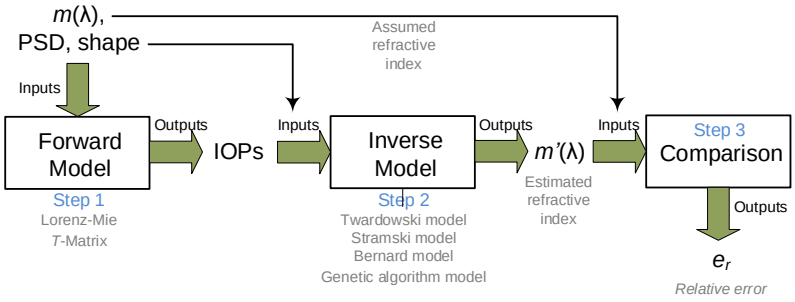

Figure 2. Procedure to analyze the accuracy of the inverse models.

as separate variables using only the absorption and attenuation efficiency factors and the concurrent measurement of the particle size distribution (PSD). And Bernard et al. (2001) simplified this model by replacing the Lorentzian oscillators with a simple Hilbert transform. All these methods share one thing in common, they approximate the shape of the particles as homogeneous spheres. Meyer (1979) first and Bernard et al. (2009) later suggested that two-layered spherical geometry models reproduce more accurately the measured algal angular scattering properties. Finally, a combination of a genetic algorithm with the Lorenz-Mie and T-Matrix approaches was used by Sánchez et al. (2014), thereby allowing more complex structures than simple homogeneous or coated spheres. A genetic algorithm is a search heuristic for optimization problems that simulates the process of natural selection using inheritance, mutation, selection, and crossover between different possible solutions. Again, this method only requires the measured attenuation and scattering coefficients, and the PSD to find the complex refractive index. This later method is much slower than the previous ones (in particular, for non-spherical particles), but it can provide very accurate estimations.

In this paper, the refractive index retrieval models mentioned above are reviewed and tested against simulated data in order to analyze their accuracy when modeling real (and usually complex-shaped) particles suspended in water such as phytoplankton. The comparison has been done following the three steps presented in Fig. 2. First, the forward models (basically, Lorenz-Mie and T-Matrix) are used to obtain the inherent optical properties (IOPs) of a selected configuration (using as inputs the assumed wavelength-dependent refractive index, $m(\lambda)$, the PSD and the particle shape). Then, the inverse models (described above) are used to estimate the refractive index using the IOPs obtained in the first step along with the PSD and the particle shape. Finally, the estimated refractive index is compared with the assumed one to obtain the accuracy of the inverse model.

The simulated examples are implemented using complex refractive indices and PSDs similar to those found in nature for phytoplankton species. Since phytoplankton particles exhibit a wide variety of shapes, each example has been provided with a different outline, accounting for a homogeneous sphere, a coated sphere and a homogeneous cylinder. None of these idealized models is an exact representation of a real algae presenting cell walls, chloroplasts, vacuole, nucleus and other internal

organelles, each with its own optical properties. However, they can be considered a first approximation suitable for the purposes of the tests presented in this contribution.

It must also be noted that the models are fundamentally different. The model developed by Twardowski et al. (2001) is intended to be used for entire particle populations that are assumed to follow a power-law size distribution while the other models are developed for single phytoplankton cultures (or dominance of one particular phytoplankton species) and require the concurrent measurement of the size distribution. And, besides, such bio-optical models are compared with a numeric method (i.e., the genetic algorithm) in the same conditions. On the other hand, the methodology applied in this contribution allows to obtain an objective comparison of the results of the different methods in those occasions where it is not clear which methodology is most suitable, and therefore, interesting for the ocean optics community.

In order to establish the foundations of the work presented in this paper, Section 2 reviews the formulation to obtain the IOPs from Lorenz-Mie and T-Matrix characterizations (that perform the forward calculations) for polydispersed algal assemblages. In Section 3, a review of the different inverse approximations to retrieve the refractive index is described. In Section 4, all the models are used to retrieve the refractive index of three assumed particles in polydisperse assemblages. Section 5 discusses the results and finally, the conclusions are outlined in Section 6.

2 Model Theory

2.1 Size Distributions and Polydispersions

Algal assemblages are typically polydispersed with regard to size, and can be described by a PSD $F(D)$, where D is the particle diameter, and $F(D)d(D)$ is the number of particles per unit volume in the size range $D \pm 1/2d(D)$ (Bricaud and Morel, 1986). Using absorption as an example (analogous expressions may be used for the other IOPs, that is, those related with light extinction and scattering), the absorption efficiency factor representing the mean of a size distribution can be described with (Bricaud and Morel, 1986):

$$\bar{Q}_a(\lambda) = \frac{\int_0^\infty Q_a(\lambda, D) F(D) D^2 d(D)}{\int_0^\infty F(D) D^2 d(D)}. \tag{1}$$

where λ denotes the wavelength. The total absorbed power per unit incident irradiance and unit volume of water, i.e., the absorption coefficient, is then given by either:

$$a(\lambda) = \frac{\pi}{4} \int_0^\infty Q_a(\lambda, D) F(D) D^2 d(D) \qquad \left[m^{-1}\right], \tag{2}$$

or, if the result of Eq. (1) is used:

$$a(\lambda) = \frac{\pi}{4}\bar{Q}_a(\lambda)\int_0^\infty F(D)D^2 d(D) \qquad \left[m^{-1}\right]. \tag{3}$$

2.2 Inherent Optical Properties

Lorenz-Mie and T-Matrix theories are powerful methods to formulate an analytical solution to electromagnetic scattering by spherical and non-spherical particles. Both rely on the expansion of the incoming light into spherical harmonics and use an intensive formulation to compute the coefficients that link the incident field with the scattered and transmitted ones. The complete Lorenz-Mie derivation is reviewed by Bohren and Huffman (1998), and the T-Matrix approach is described by Mischenko et al. (1996). Both theories provide the particle specific optical properties, i.e., the extinction, scattering and absorption cross sections (which describe the area of the incident-beam intensity converted to extincted, scattered or absorbed light), C_e, C_s and C_a respectively. The relationship between wavelength-dependent efficiency factors and cross sections is:

$$Q_x(\lambda) = \frac{C_x(\lambda)}{G}, \tag{4}$$

being x any of the subindices e, s or a to denote extinction, scattering or absorbtion, and G the geometric cross section of the particle. The obtained cross sections from Lorenz-Mie and T-Matrix (size-averaged in polydisperse concentrations as described above) can also be used to compute the extinction, scattering and absorption coefficients ($c(\lambda)$, $b(\lambda)$ and $a(\lambda)$ respectively) as (Quirantes and Bernard, 2006):

$$c(\lambda) = N \cdot \bar{C}_e(\lambda) \qquad \left[m^{-1}\right], \tag{5}$$

$$b(\lambda) = N \cdot \bar{C}_s(\lambda) \qquad \left[m^{-1}\right], \tag{6}$$

$$a(\lambda) = N \cdot \bar{C}_a(\lambda) \qquad \left[m^{-1}\right], \tag{7}$$

where N denotes the number of particles per unit volume. The relationship between the three parameters is:

$$c(\lambda) = a(\lambda) + b(\lambda) \qquad \left[m^{-1}\right]. \tag{8}$$

Scattering can be further characterized in terms of the angular distribution of the scattered light using the volume scattering function (β) as (Mobley, 1994):

$$\beta(\Psi,\lambda) = \widetilde{\beta}(\Psi,\lambda)\cdot b(\lambda) \qquad \left[m^{-1}sr^{-1}\right]. \tag{9}$$

Ψ is the scattering angle (i.e., the angle between the incident and scattered beams) and $\widetilde{\beta}(\Psi,\lambda)$ is the scattering phase function and the first parameter of the Stokes scattering matrix (or Mueller matrix). This matrix transforms the Stokes parameters of the incident light into those of the scattered light and it is obtained with the Lorenz-Mie and T-Matrix formulation when the physical characteristics of the particles are known. The integral scattering in all directions, assuming azimuthal symmetry, retrieves the total scattering coefficient b:

$$b(\lambda) = 2\pi \int_0^\pi \beta(\Psi,\lambda) sin(\Psi) d\Psi \qquad \left[m^{-1}\right], \tag{10}$$

which can be partitioned into its forward and backward components (b_f and b_b respectively) by limiting the integration bounds from 0 to $\pi/2$ and from $\pi/2$ to π respectively. The backscatter fraction, defined by:

$$B_b(\lambda) = \frac{b_b(\lambda)}{b(\lambda)}. \tag{11}$$

gives the fraction of scattered light that is deflected through the scattering angles beyond $\pi/2$. Given Eq. (9) and Eq. (10), the normalization condition for the volume scattering phase function is:

$$2\pi \int_0^\pi \widetilde{\beta}(\Psi,\lambda) sin(\Psi) d\Psi = 1. \tag{12}$$

This normalization implies that the backscatter fraction can be computed using the volume scattering phase function as:

$$B_b(\Psi,\lambda) = 2\pi \int_{\frac{\pi}{2}}^\pi \widetilde{\beta}(\Psi,\lambda) sin(\Psi) d\Psi. \tag{13}$$

The 2π factor used in Eq. (10), Eq. (12) and Eq. (13) (which comes naturally from integration with respect to the azimuth angle) is different from the $1/2$ factor used by Mischenko et al. (1996); Mischenko and Travis (1998); Wiscombe and Grams (1976); Mugnai and Wiscombe (1986) (where the integration of phase function is normalized to 4π, representing the total solid angle over entire sphere), but used by Twardowski et al. (2001), Bohren and Huffman (1998), and most of the literature in Ocean Optics (Mobley, 1994), and therefore, applied here.

Table 1. Summary of the refractive index retrieval models

Inverse models	Inputs	Outputs	Type of particles	Assumptions	Equations
Twardowski Model	B_b, ξ	n	Homogeneous spheres	$k = 0.005$, Power-law PSD, $gamma = \chi - 3$	(9), (15)
Stramski Model	PSD, a and c (or Q_a and Q_c)	n, k	Homogeneous spheres	$\alpha \gg 1$, $n - 1 \ll 1$, $k \ll 1$	(13), (16), (17), (18), (19)
Bernard Model	a, PSD	n_{chlor}, k_{chlor}	Coated spheres	n_{cyto}, k_{cyto}, V_V, $1 + \epsilon$	(16), (17), (20), (21)
Genetic Algorithm Model	a, c, PSD	n, k	Homogeneous and coated spheres, spheroids, cylinders and Chebyshev particles	Particles with axial symmetry	(2), (3), (22)

3 Review of Refractive Index Retrieval Models

In this section, a review of the different approximations to retrieve the refractive index (inverse models) is presented. Each method is named using the surname of the lead author of the publication. In order to make the understanding of this section easier, Table 1 shows, for each model, their inputs and outputs, type of particles, as well as the assumptions of the model and the equations used.

The complex refractive index $m(\lambda)$ is defined as:

$$m(\lambda) = n(\lambda) + ik(\lambda), \tag{14}$$

where the real part $n(\lambda)$ determines the phase velocity of the propagating wave, and the imaginary part $k(\lambda)$ determines the flux decay. The sign of the complex part is a matter of convention (it can also be defined with a negative sign). The notation above corresponds to waves with time evolution given by $e^{-i\omega t}$. Note that this paper assumes effective refractive indices relative to seawater, which has a constant value of $m_{water} = 1.334 + i0$ (Hale and Querry, 1973). Absolute values can be recovered using $m_a = m \times m_{water}$.

3.1 The Twardowski Model

The Twardowski model, presented by Twardowski et al. (2001), is based on Volz (1954) as cited in van de Hulst (1957). It is derived using the Lorenz-Mie theory and the relationship between the particulate spectral attenuation ($c_P(\lambda)$) and the size distribution to retrieve the bulk particulate refractive index from $in\ situ$ optical measurements. In particular, assumes that $\gamma = \xi - 3$ (γ is the hyperbolic slope of the attenuation coefficient and ξ is the power-law slope of the PSD). It only considers power-law distributions that fulfill the conditions $2.5 \leq \xi \leq 4.5$ and $0 \leq B_b \leq 0.03$. The bulk refractive index is obtained using a polynomial fit to the output of Lorenz-Mie calculations as:

$$\hat{n}\left(B_b, \gamma\right) = 1 + B_b^{0.5377+0.4867\gamma^2}\left(1.4676 + 2.2950\gamma^2 + 2.3113\gamma^4\right). \tag{15}$$

This formulation is only exact for particles which size spans from 0 to infinity with a constant absorption along wavelength (k is held constant at 0.005) and are homogeneous spheres. It was first tested by Boss et al. (2001a) and refined in Boss et al. (2001b). It must be noted that the model is consistent with the measurements obtained from an AC9 with the scattering coefficient b serving as integrated scattering from 0.93 to 180 degrees, which must be considered in Eq. (13). Even though this was not firstly considered in the calculations in Twardowski et al. (2001), it was taken into account in Boss et al. (2004), but the regression was not recomputed.

3.2 The Stramski Model

This model is based on the methods presented by Stramski et al. (1988), which is an extension of that developed by Bricaud and Morel (1986). It is based on the ADA, first described in van de Hulst (1957). The ADA offers approximations to the absorption and attenuation optical efficiency factors using relatively simple algebraic formulae, based on the assumptions that the particle is large relative to wavelength ($\alpha = \frac{\pi D}{\lambda} \gg 1$) and the refractive index is small ($n - 1 \ll 1$ and $k \ll 1$). This method allows the effects of the real and imaginary refractive indices on absorption and scattering to be decoupled. Assuming homogeneous geometry, the ADA expression for the absorption efficiency factor is given by:

$$Q_a\left(\rho'\right) = 1 + \frac{2e^{-\rho'}}{\rho'} + 2\frac{e^{-\rho'} - 1}{\rho'^2}, \tag{16}$$

where $\rho' = 4\alpha k$ is the absorption optical thickness. Eq. (3) and Eq. (16) are then used iteratively to determine the homogeneous imaginary part of the refractive index ($k(\lambda)$) in conjunction with measured algal absorption and PSD data. According to the Ketteler-Helmholtz theory of anomalous dispersion (van de Hulst, 1957), a variation in k induces variations in n, quantified with a series of oscillators (representing discrete absorption bands) based on the Lorentz-Lorentz equations (Stram-

ski et al., 1988; Bricaud and Morel, 1986). These spectral variations (denoted as $\Delta n(\lambda)$) vary around a central part of the real refractive index $1+\epsilon$. Thus:

$$n(\lambda) = 1 + \epsilon + \Delta n(\lambda). \tag{17}$$

The central value $1+\epsilon$ is estimated by computing the nonabsorbing equivalent population attenuation efficiency factor ($\bar{Q}_c^{NAE}$) at those wavelengths where $\Delta n(\lambda_\epsilon) = 0$. Considering polydispersion, this is done according to:

$$\bar{Q}_c^{NAE}(\bar{\rho}) = \frac{\int_0^\infty Q_c(\rho) F(\rho) \rho^2 d(\rho)}{\int_0^\infty F(\rho) \rho^2 d(\rho)}, \tag{18}$$

where $\rho = 2\alpha(n-1)$, $F(\rho)$ is obtained from the experimental size distribution by the replacement of D by ρ and $Q_c(\rho)$ from the van de Hulst's formula assuming $\xi = 0$ (van de Hulst, 1957):

$$Q_c(\rho) = 2 - \frac{4}{\rho} sin\rho + \frac{4}{\rho^2}(1 - cos\rho). \tag{19}$$

The exact value of ϵ is indicated by such $\bar{Q}_c^{NAE}(\bar{\rho})$ that it equals $\bar{Q}_c(\lambda_\epsilon)$.

This methodology was latterly simplified by Bernard et al. (2001, 2009) by using the Kramers-Kronig relations to compute the spectral variations in the real part of the refractive index instead the Lorentzian oscillators. The Kramers-Kronig relations describe the mutual dependence of the real and imaginary parts of the refractive index through dispersion, as does Ketteler-Helmholtz theory, but they are more simply applied than the tedious and sometimes inaccurate use of summed oscillators (the real part is the Hilbert transform of the imaginary part, van de Hulst, 1957).

3.3 The Bernard Model

Meyer (1979) and Bernard et al. (2009) suggested that two-layered spherical geometry models reproduce more accurately the measured algal angular scattering properties. In Bernard et al. (2009), the outer layer accounts for the chloroplast and the inner layer for the cytoplasm. Refractive index values are assumed for the cytoplasm, with a spectral imaginary part modelled as:

$$k_{cyto}(\lambda) = k_{cyto}(400) e^{[-0.01(\lambda - 400)]}, \tag{20}$$

where $k_{cyto}(400) = 0.0005$. The real refractive index spectra for the cytoplasm, $n_{cyto}(\lambda)$, is obtained using the Hilbert transform (absorption has an influence on scattering and attenuation, expressed through the Kramers-Kronig relations) and Eq. (17) with $1+\epsilon = 1.02$. Using the $k_{cyto}(\lambda)$ of Eq. (20), volume equivalent $k_{chlor}(\lambda)$ are determined using the Gladstone-Dale formulation given by:

$$k_{chlor}(\lambda) = \frac{k_h(\lambda) - k_{cyto}(\lambda) V_V}{1 - V_V}, \tag{21}$$

where $k_h(\lambda)$ is the imaginary part of the refractive index considering homogeneous cells and obtained using Eq. (16), and V_V is the relative chloroplast volume. According to Bernard et al. (2009), a V_V value of 20% can be considered as a first approximation for a spherical algal geometry, although higher values should be considered for the large celled dinoflagellate and cryptophyte samples. Other previous studies have employed relative chloroplast volumes of V_V = 41% (Zaneveld and Kitchen, 1995), V_V = 58% (Latimer, 1984), and V_V = 27% to 66% (Bricaud et al., 1992). The real refractive index spectra for the chloroplast $n_{chlor}(\lambda)$ is then similarly generated with a Hilbert transform and Eq. (17) with assumed $1+\epsilon$ values between 1.044 and 1.14 depending upon the sample.

3.4 The Genetic Algorithm Model

The model presented by Sánchez et al. (2014) uses a genetic algorithm to find the refractive index that produces the desired scattering and absorption coefficients (a and b) when using the Lorenz-Mie or T-Matrix approaches with the measured PSD. The methodology of the algorithm can be summarized as follows (see Fig. 3). First, a random vector of solutions is generated for a specific wavelength ($[m_1(\lambda_i)$, $m_2(\lambda_i)$, ..., $m_n(\lambda_i)]$, where λ_i denotes the selected wavelength and $m_1, m_2, ..., m_n$ the complex refractive indices). If possible, the search space can be bounded in order to maximize the algorithm success. Then, the complete vector is evaluated by the fitness function. This is done by computing the a and b coefficients corresponding to each refractive index (using the Lorenz-Mie or T-Matrix formulation and Eq. (6) – Eq. (7)) and evaluating the weighted euclidean distance between the calculated and desired coefficients. This can be obtained, for instance, as:

$$e_a(\lambda_i) = |20log(\hat{a}_k(\lambda_i)) - 20log(a_m(\lambda_i))|, \tag{22}$$

where a_k is the calculated absorption coefficient of the n_k refractive index, a_m is the desired (or measured) attenuation coefficient, and e_a is the committed error for the absorption coefficient. Using logarithmic values allows a suitable weighting factor when dealing with small errors over small coefficients. The same equation can be used for the scattering coefficient. Both results are finally combined using the quadratic mean, obtaining a single evaluation value that the algorithm tries to minimize.

After the evaluation, the algorithm may stop if either a maximum number of generations (each generation is a new vector of solutions) or a satisfactory fitness level have been reached. If the convergence condition is not fulfilled, the best solutions are selected and separated. Part of this elite is then recombined (crossover) and randomly mutated to provide genetic diversity and broaden the search space (crossover and mutation introduce the diversity needed to ensure that the entire sample space is reachable and avoid becoming stuck at suboptimal solutions, Greenhalgh and Marshall, 2000). The new set of solutions is re-evaluated and inserted again into the solutions' vector, which

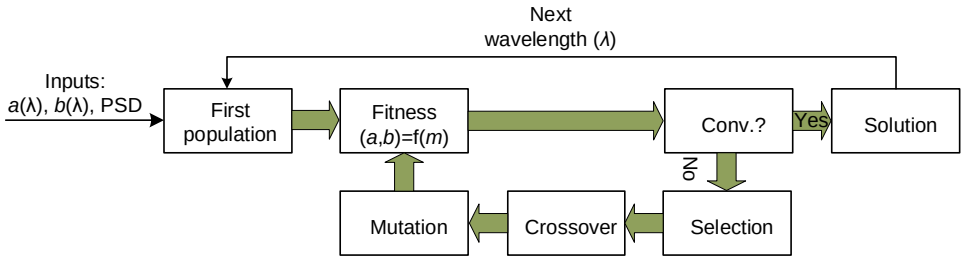

Figure 3. Flow chart of the genetic algorithm.

completes the cycle. After convergence is achieved, the algorithm presents the best solution it has been able to find.

Since Lorenz-Mie and T-Matrix algorithms can only be executed for single wavelengths, and the refractive index is also wavelength dependent (with different values at different wavelengths), the genetic algorithm performs the search procedure at a single wavelength each time. After each convergence, the process starts again with the next wavelength-dependent values, eventually obtaining the complete complex-refractive-index signature.

The main advantage of this model is that it can be easily adapted to different Lorenz-Mie or T-Matrix codes, as for instance those developed for homogeneous spheres, coated spheres, cylinders, etc. Besides it can also be easily combined with other models to improve the results. On the other hand, it must be noted, that some inversions could be ill-posed. A constrained optimization problem is considered to be well-posed in the sense of Haddamard if (a) a solution exists, (b) the solution is unique and (c) the solution is well-behaved, i.e. varies continuously with the problem parameters. An ill-posed problem fails to satisfy one or more of the aforementioned criteria (Bhandarkar et al., 1994). In that case, techniques such as regularization methods can be applied to improve the results (Mera et al., 2004).

4 Experimental Simulations

The models described in the previous section are used here to retrieve the refractive index of well-known particles in order to determine their accuracy by means of the averaged relative error defined as

$$e_{rx}\,(\%) = \frac{1}{N}\sum_{n=1}^{N}\left|\frac{x'(\lambda_n)}{x(\lambda_n)} - 1\right| \times 100, \tag{23}$$

where x' accounts for the estimated real part of the refractive index as $n'(\lambda) - 1$ (the unity is subtracted to only consider the decimals) or the estimated imaginary part of the refractive index as $k'(\lambda)$, and x accounts for the assumed real part of the refractive index as $n(\lambda) - 1$ or the assumed

imaginary part of the refractive index as $k(\lambda)$. For the volume scattering function, error is also averaged with respect to its angular contribution as:

$$e_{rVSF}\,(\%) = \frac{1}{N \cdot M} \sum_{n=1}^{N} \sum_{m=1}^{M} \left| \frac{VSF'(\lambda_n, \theta_m)}{VSF(\lambda_n, \theta_m)} - 1 \right| \times 100, \tag{24}$$

To this end, Subsection 4.1 deals with a simple spherical and homogeneous particle and presents the results provided by the Twardowski, Stramski and Genetic Algorithm models. Such particles, however, are not a fair representation of phytoplankton particles. First, because eukaryotic phytoplankton cells are heterogeneous particles with membrane systems and intracellular organelles, and second, because most of the phytoplankton species are not spherical. As stated by Bernard et al. (2009), the spherical structure mainly fails in the description of the backward scattering and suggests a two-layered spherical geometry as the simplest possible heterogeneous structure capable of reproducing measured algal angular scattering properties. In consequence, Subsection 4.2 presents a coated sphere as the assumed particle and presents the estimated refractive indices provided by the genetic algorithm model, the Bernard model and a combination of both. Finally, Subsection 4.3 uses a cylindrical shape particle with a homogeneous refractive index. This shape was selected to be different from a sphere and similar to that of some species of phytoplankton (as for instance, the diatom $Thalassiosira\ pseudonana$). Although this assumed model does not exactly reproduce the same optical behavior as the actual phytoplankton particle (the micro-details of the cells are neglected), it can serve as a first approximation. Refractive index estimations provided by the combination of the Genetic Algorithm with the Bernard model for coated spheres and the Genetic Algorithm alone are shown.

4.1 Spherical-Shaped Homogeneous Particles

A concentration of 100 spherical particles per mm^3 presenting the PSD of Fig. 4a (based on a power-law distribution -or Junge-type- with 51 points, $R_{min} = 0.7\ um$, $R_{max} = 12.1\ um$, a slope parameter $\xi = 3$, effective radius $r_{eff} = 4\ \mu m$ and effective variance $v_{eff} = 0.6$), along with the assumed complex refractive index of Fig. 4b, was simulated using the Lorenz-Mie scattering theory (Bohren and Huffman, 1998). In particular, the BHMIE code, originally from Bohren and Huffman and modified by B.T. Draine, was used as a Forward Model (additional features were added, such as polydispersion and the computation of the Stokes scattering matrix). The computed IOPs from this forward model, i.e. the $a(\lambda)$, $b(\lambda)$ and $c(\lambda)$ coefficients are shown in Fig. 5a. As can be observed, the concentration was selected in order to obtain IOP coefficients similar to those measured by Twardowski et al. (2001) and Stramski et al. (2001). Although the power-law distribution is not a realistic distribution for single phytoplankton species, it is a fairly good approximation of natural-water composition (even with anomalous natural conditions such as a phytoplankton bloom), as there is always a strong background contribution to the PSD (Twardowski et al., 2001). Besides, it is the only distri-

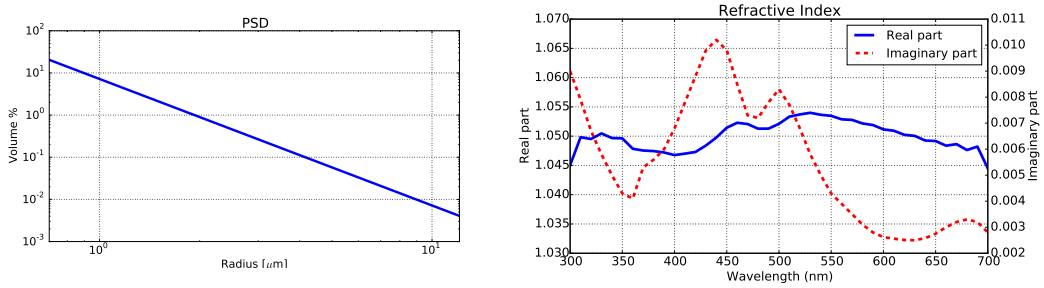

(a) (b)

Figure 4. (a) PSD of the test run with spherical-shaped homogeneous particles. (b) Assumed complex refractive-index signature of the example with spherical-shaped homogeneous particles.

bution that can be used in the Twardowski model, and therefore, used here. The complex refractive index of Fig. 4b was synthetically generated using imaginary values similar to those presented in Bernard et al. (2009) for phytoplankton species (derived from sample algal assemblages and considering homogeneous spheres). The dependence of the real on the imaginary part of the refractive index can be found in the Kramers-Kronig relations (Bernard et al., 2001, 2009; Bricaud and Morel, 1986; van de Hulst, 1957), which allow the spectral variations in the real refractive index to be calculated as a Hilbert transform of the imaginary refractive index. The central part of the real refractive index was selected as $1 + \epsilon = 1.05$ (for phytoplankton it typically ranges from 1.02 to 1.15, relative to water, as stated in Morel, 1973, Carder et al., 1974, Aas, 1996, Bernard et al., 2001). The effects due to normal dispersion, as described in Aas (1996), have not been considered. As can be seen, the imaginary part presents three peak values, at 440, 500 and 680 nm (corresponding to the chlorophyll absorption wavelengths), and, as expected, a similar shape is propagated to the absorption coefficient spectra, $a(\lambda)$, of Fig. 5a. The volume scattering function is shown in Fig. 5b. Only three wavelengths (300, 500 and 700 nm) are plotted using intense colors, while the rest of wavelengths between 300 and 700 nm in steps of 10 nm are plotted in light grey. As expected (since particles are relatively large regarding to wavelength), the scattering is mainly focused in the forward direction (between 0 and 10 degrees) and smoothly decreases in the backward direction.

4.1.1 The Twardowski Model

Eq. (15) was applied to this example obtaining the results shown in Fig. 6a. To this end, $\gamma = 0$ since the slope parameter of the PSD $\xi = 3$, and the backscatter fraction was computed with Eq. (13) using the volume scattering phase function values given by the modified BHMIE code. As can be seen, for the real part, this model obtains a curve shape similar to the assumed complex refractive index, but with a slight negative offset, presenting an averaged relative error of 42%. Since this model assumes a constant imaginary refractive index value of 0.005, the averaged relative error with the assumed imaginary part of the refractive index is 44%. It must be noted that the Twardowski model

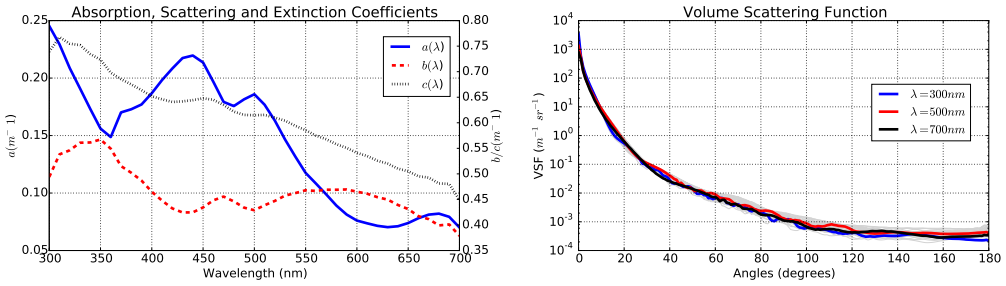

(a) (b)

Figure 5. (a) Absorption (a), scattering (b) and extinction (c) coefficients of the example with spherical-shaped homogeneous particles, and (b) the volume scattering function.

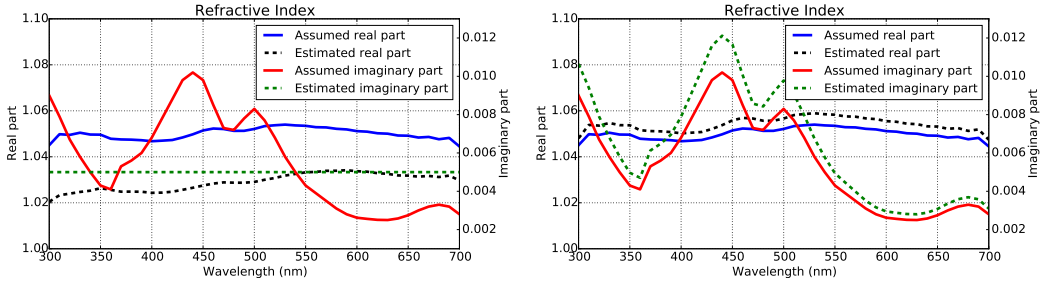

(a) (b)

Figure 6. (a) Assumed and estimated refractive indices using the model of Twardowski et al. (2001). (b) Assumed and estimated refractive indices using the Stramski model.

was designed for a bulk oceanic distribution presenting different physical properties than those of isolated species of phytoplankton (e.g. index of refraction, shape, etc.), and therefore, it is used here in a different scenario than it was designed to.

4.1.2 The Stramski Model

The results obtained with this model are shown in Fig. 6b. As can be seen, this model overestimates both real and imaginary parts on all the analysed spectra, showing an averaged relative error of 0.4% for the real part and a 15% for the imaginary part. It should be remembered that the imaginary part of the refractive index, k_h, is calculated with the ADA, known to give errors of $\sim$10% in comparison to Lorenz-Mie theory (Bernard et al., 2009), and some discrepancies can therefore be expected between ADA and Aden-Kerker derived values (Aden and Kerker, 1951).

4.1.3 Genetic Algorithm

In order to implement the genetic algorithm described in Section 3.4, the tools provided by the DEAP (Distributed Evolutionary Algorithms in Python) and SCOOP (Scalable COncurrent Operations in

Python) frameworks to develop evolutionary algorithms and parallel task distribution respectively, were used (Fortin et al., 2012; Hold-Geoffroy et al., 2014). The fitness function was implemented using the fast subroutines of BHMIE to compute the absorption and scattering properties of homogeneous spheres. The coefficients a and b of Fig. 5a were used as inputs of the genetic algorithm model to estimate the assumed complex refractive index and bounding conditions were applied to facilitate the convergence (typical values for the real part of the phytoplankton refractive indices fall within 1.02 and 1.15 relative to water, and the bulk value of the imaginary part is always below 0.02). The genetic algorithm was configured with a vector of 2000 solutions over 10 generations and 50% and 20% of probability of crossover and mutation respectively, obtaining the estimated values shown in Fig. 7a. The good agreement between the assumed complex-refractive-index values and the estimated ones (an averaged relative error of 0.004% for the real part and 0.24% for the imaginary part is obtained, presenting thus the best results in this first example) shows that it is possible to perform accurate estimations with a genetic algorithm. It must be noted that the number of generations needed to have a suitable convergence strongly depends on the length of the initial-solution vector and the cross-over and mutation percentages, among other parameters of the Genetic Algorithm. In this particular case, using the described parameters, no significant improvement is generally found beyond the tenth generation.

One disadvantage of the genetic algorithms is that they are relatively slow and require more computation time than other optimization algorithms, since they need to execute the fitness function many more times. Other optimization algorithms were also applied to determine if similar results can be obtained with a significant reduction of the computation time. However, since none of them led to any meaningful improvement, they are not introduced here in a deeper detail. As an example, Fig. 7b shows the results obtained with the much faster Broyden-Fletcher-Goldfarb-Shanno (BFGS) algorithm (BFGS is an iterative method for solving unconstrained nonlinear optimization problems, Zhu et al., 1997), executed using the same bounding conditions as in the genetic algorithm case. In this case, only 224 seconds (less than 4 minutes) were needed in front of the 97 minutes used by the genetic algorithm, both in a PC with an Intel Core i7 processor at 3.2 GHz, a 16-GB RAM and running a Windows 8.1. However, although the results are quite satisfactory in general, some of the wavelengths present a significant error in the real part (mainly, between 550 and 600 nm, and above 680 nm). The averaged relative error is 0.073% for the real part and 0.72% for the imaginary part. Other optimization algorithms, such as the conjugated gradient algorithm (Nocedal and Wright, 1999), were also tested. The results (not shown), exhibited a worse accuracy than the BFGS, showing that the genetic algorithm is probably the optimal method to solve this problem in terms of accuracy (but not in terms of time).

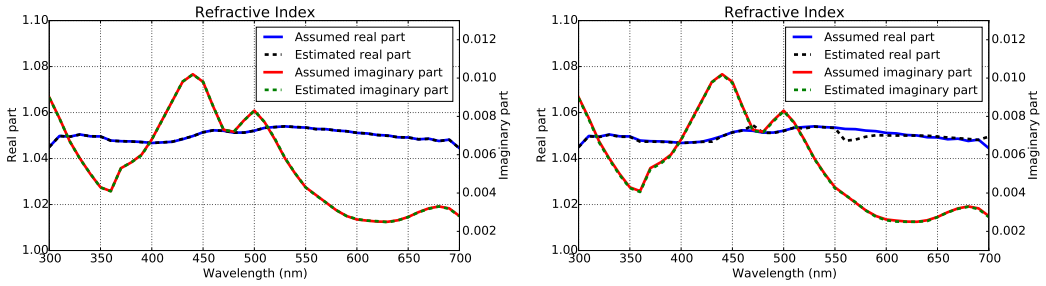

(a) (b)

Figure 7. (a) Assumed and estimated refractive indices using the Genetic Algorithm presented in this paper. Note that assumed and estimated values are on top of each other. (b) Assumed and estimated refractive indices using the BFGS algorithm.

4.2 Spherical-Shaped Coated Particles

In order to use the IOPs of a two-layered spherical particle that emulates actual phytoplankton properties, its complex refractive index was generated using the description presented in Bernard et al. (2009). The imaginary refractive index of the inner cytoplasm was obtained using Eq. (20) and its real one using the Hilbert transform (Hahn, 1996) and Eq. (17) with $1+\epsilon = 1.02$. The imaginary refractive index of the outer chloroplast was obtained using Eq. (21), with $V_V = 30\%$ (since it is a value between that assumed by Bernard et al., 2009, and previous works), and its real one using the Hilbert transform and Eq. (17) with $1+\epsilon = 1.1$. Fig. 8a and Fig. 8b show the results for the real and imaginary parts respectively (assumed values). In this example, instead of using a PSD describing a power-law function (as in Fig. 4a), the PSD of an isolated culture was simulated with a concentration of 40 particles per mm^3 ($R_{min} = 0.7\ um$, $R_{max} = 12.1\ um$ and using 31 points), as seen in Fig. 9. It must be noted that the PSD denotes the external radius (the inner one can be calculated using the V_V value). Using this PSD with the previous refractive indices in the BART code from A. Quirantes (Quirantes, 2005) (a Forward Model based on the Aden-Kerker theory to calculate light-scattering properties for coated spherical particles), the absorption, scattering and extinction coefficients of Fig. 10a, and the volume scattering function of Fig. 10b were obtained.

Below, the IOPs presented above are used to estimate their complex refractive indices. First, this is done using the genetic algorithm in order to see if a basic shape such as a homogeneous sphere is useful when modelling more complex particles. If coated particle models better characterize the optical properties of general phytoplankton species, as stated in Bernard et al. (2009), this can be used to estimate the error committed when using spheres. Then, the inner and the outer complex refractive indices of the original particle are retrieved using the Bernard model for coated particles. Finally, a combination of the genetic algorithm and the Bernard model is applied to improve the previous results. Note that the Twardowski model is not applied to avoid unfair (i.e., inconsistent)

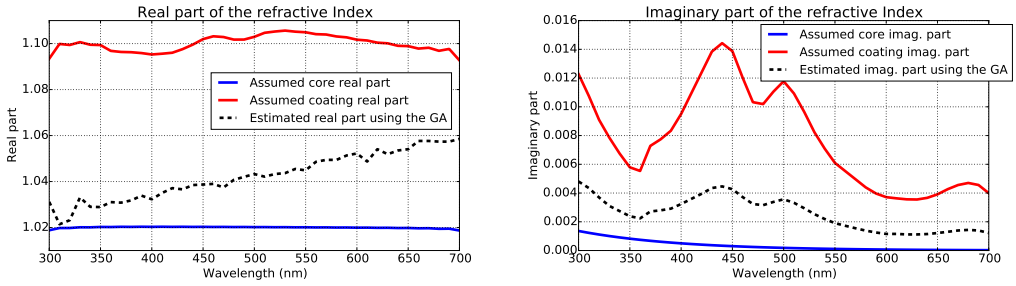

(a) (b)

Figure 8. (a) Assumed real refractive-index signatures for the inner and outer layers and estimated real refractive-index signature using the genetic algorithm model. (b) Assumed imaginary refractive-index signatures for the inner and outer layers and estimated imaginary refractive-index signature using the genetic algorithm model.

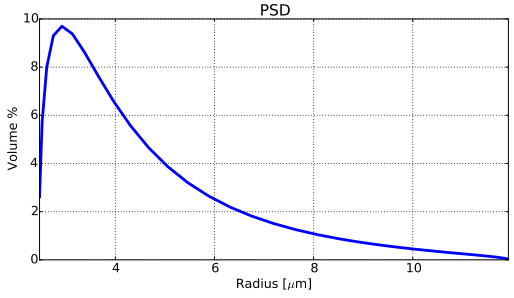

Figure 9. PSD that simulates a an isolated culture.

comparisons with the other methods (it was designed to be used with entire particle populations that are assumed to follow a power-law size distribution).

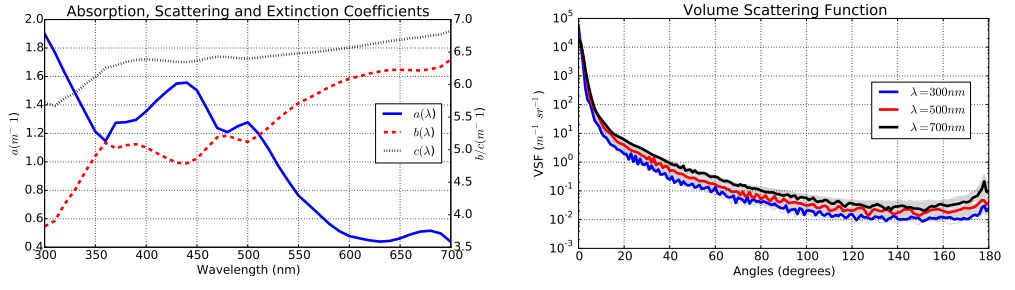

(a) (b)

Figure 10. (a) Absorption (a), scattering (b) and extinction (c) coefficients of the coated-particle example, and (b) the volume scattering function.

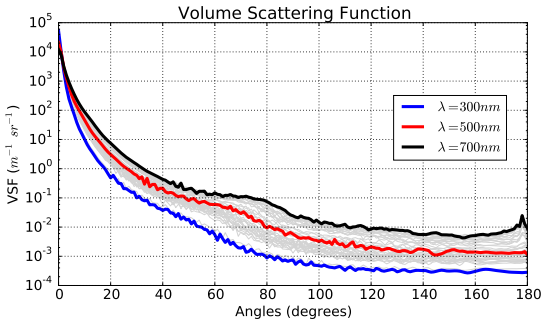

Figure 11. Volume scattering function using the estimated refractive index in the spherical-Shaped coated-particle example.

4.2.1 The Genetic Algorithm

The genetic algorithm model to retrieve the refractive index of spherical-shaped homogeneous particles was applied in order to measure the error committed in such approximation. The same configuration as in the previous example was used (an initial vector of 2000 solutions over 10 generations and 50% and 20% of probabilities for crossovers and mutations respectively). The estimated complex refractive index is shown in Fig. 8a and Fig. 8b. As it can be seen, both real and imaginary parts present values between the inner and the outer real and imaginary parts. The volume scattering function generated by the homogeneous particles, as seen in Fig. 11 (obtained by means of a forward model, i.e., Lorenz-Mie, using the estimated complex refractive index and the PSD of Fig. 9 as inputs), shows that this model presents similar values in the forward scattering but completely underestimates the backscattering, presenting values far below those of Fig. 10b. This example demonstrates that the common characterization using homogeneous spheres is not a suitable methodology when dealing with complex particles. Even though it is not a surprising result (this is well known and has been discussed for years, by Bohren and Huffman, 1998, in the atmospheric literature, and by Stramski et al., 2004, Clavano et al., 2007, Dall'Olmo et al., 2009, and Bernard et al., 2009, in the oceanic literature), a comparison between the two volume scattering functions manifests that the backscattering can exhibit errors up to one order of magnitude.

4.2.2 The Bernard Model

The Bernard model of Section 3.3 was used to estimate the complex refractive index of the two-layered particle. Figure 12a shows the assumed and estimated real part of the inner and outer layers and Figure 12b shows the assumed and estimated imaginary parts. As expected, the inner refractive index is well estimated (since the same equation is used for both generation and retrieval), but the outer refractive index does not present an accurate agreement. In particular, the imaginary part is significantly underestimated, with an averaged relative error of 51%. On the other hand, the sim-

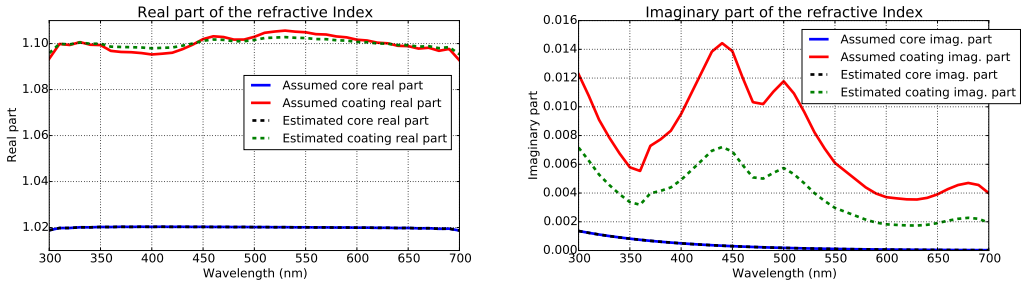

(a) (b)

Figure 12. (a) Assumed and estimated real part of the refractive indices for the inner and outer layers using the Bernard model. (b) Assumed and estimated imaginary part of the refractive indices for the inner and outer layers using the Bernard model.

ulation of the estimated refractive indices in coated spheres produce a volume scattering function which is in a better agreement with that of Fig. 10b than the volume scattering function produced by the homogeneous spherical particle (the volume scattering function figure has not been added in this case since errors are not apparent on the graph; a more detailed analysis is done in Section 5).

4.2.3 The Bernard Model combined with Genetic Algorithm

In order to improve the results presented by the Bernard model in the previous subsection, the genetic algorithm, which showed a reasonable performance when applied to homogeneous spherical particles, could be coupled to the BART code (instead the BHMIE code) to try to estimate the two complex refractive indices. However, results would hardly be constrained since the solution has more degrees of freedom (the two refractive indices with real and imaginary parts each, that is, four dimensions) than the information data (the attenuation and scattering coefficients, that is, two dimensions), i.e., this is an unconstrained (ill-posed) problem. However, there is the possibility to combine the genetic algorithm with the Bernard model to increase the convergence probability. In this case, the inner refractive index is firstly estimated using the Bernard model, as it was done before, and the outer refractive index is obtained secondly with the genetic algorithm (coupled to the BART code). In this case, the genetic algorithm only has to find a solution with two dimensions (the real and imaginary parts of the outer refractive index).

This method was applied on the coated particle example (using the coefficients of Fig. 10a as input data and configured using an initial vector of 2000 solutions, 10 generations, 50% of probability for crossovers and 20% for mutations), obtaining the assumed and estimated real part of the inner and outer layers shown in Figure 13a and the assumed and estimated imaginary parts shown in Figure 13b. As it can be seen, accurate results were obtained, meaningfully improving the refractive index estimation for the outer sphere. In this particular case, an average relative error of 0.01% was obtained for the real part and a 0.14% for the imaginary part.

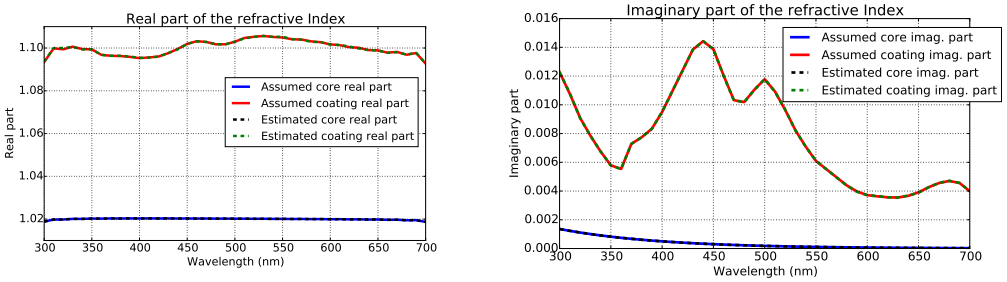

(a) (b)

Figure 13. (a) Assumed and estimated real part of the refractive indices for the inner and outer layers using the Bernard model combined with the genetic algorithm. (b) Assumed and estimated imaginary part of the refractive indices for the inner and outer layers using the Bernard model combined with the genetic algorithm. Note that in both cases, assumed and estimated values are on top of each other.

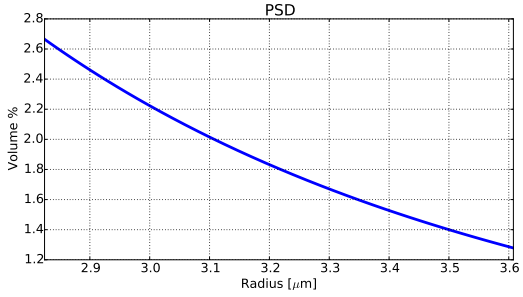

Figure 14. PSD of the cylindrical-shaped example.

4.3 Cylindrical-Shaped Particles

As a final example, a cylindrical shape particle has been chosen. As commented above, phytoplankton species usually present complex shapes, far from perfect homogeneous or coated spheres (as it is the case of the diatom $Thalassiosira\ pseudonana$). In order to find which is the most accurate model for the characterization of such complex shapes, an example considering 100 prolate cylinders per mm^3 with a diameter-to-length ratio equivalent to 0.8, the PSD of Fig. 14 (showing the radius of an equivalent volume sphere with a slope parameter $\xi = 3$, effective radius $r_{eff} = 3.2\ \mu m$ and effective variance $v_{eff} = 0.005$ resulting in $R_{min} = 0.8\ \mu m$ to $R_{max} = 3.6\ \mu m$), and the assumed refractive index of Fig. 4b was simulated using the T-Matrix algorithm (Mischenko et al., 1996; Mischenko and Travis, 1998) as a Forward Model. To this end, the code from M. Mischenko (Mischenko and Travis, 1998) for T-Matrix computations on randomly oriented, rotationally symmetric scatterers (cylinders, spheroids and Chebyshev particles) was used. The PSD presents a small effective variance for convergence limitations of the code. The assumed $a(\lambda)$, $b(\lambda)$ and $c(\lambda)$ coefficients are shown in Fig. 15a, and the volume scattering function at each wavelength is shown in Fig. 15b.

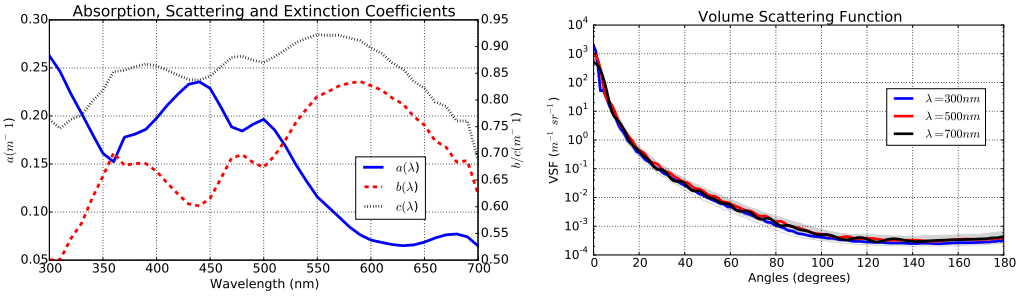

(a) (b)

Figure 15. (a) Absorption (a), scattering (b) and extinction (c) coefficients of the cylindrical-shaped example. (b) Volume scattering function of the cylindrical-shaped example.

4.3.1 The Bernard Model combined with Genetic Algorithm

Even though these simulated particles are not an exact copy of an actual phytoplankton (for the reasons commented before), the coated sphere model is used here to model the cylindrical shape to analyze their differences. As in previous examples, the assumed value was $V_V = 30\%$ (an averaged value between that assumed by Bernard et al., 2009, and previous works). Figure 16a shows the estimated real part of the inner and outer layers and Figure 16b shows the estimated imaginary parts. In this case, they cannot be compared with the assumed individual refractive index of the cylindrical particle. Instead, the IOPs obtained from the estimated refractive indices need to be computed using the forward model to analyze if this model is useful to emulate homogeneous cylinders. The volume scattering function, obtained by means of the estimated complex refractive indices and the PSD of Fig. 14 in a forward model, i.e., the T-Matrix, is shown in Fig. 17. The committed error in this last figure is noticeable even to the naked eye, especially at longer wavelengths, achieving an averaged relative error of 77%. It should be noted that these differences may decrease when using real phytoplankton, since backscattering of heterogeneous particles is different from that of homogeneous particles.

4.3.2 The Genetic Algorithm

The genetic algorithm can be combined with the T-matrix code in order to consider cylindrical shapes when estimating the inner complex refractive index. However, one simulation of cylindrical shape particles with such dimensions, using the Mischenko code, needs about 67 minutes in a computer with an i7 at 3.20 GHz and running Windows 8.1. This prevents the use of the genetic algorithm in such circumstances, since it needs to execute this simulation several hundreds of times at each wavelength in order to accurately estimate the complex refractive index. That means that several months would be required to estimate the whole refractive index spectra. To avoid that, some kind of approximations must be considered. In order to perform fast estimations, equal-volume ho-

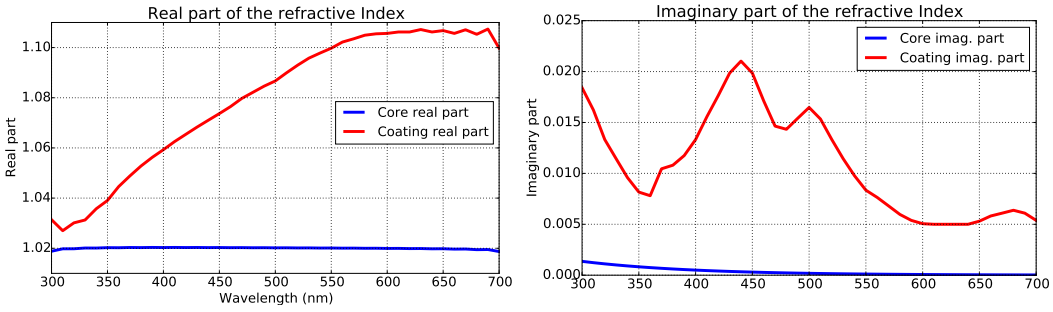

(a) (b)

Figure 16. (a) Inner and outer real part of the refractive indices using the Bernard Model combined with Genetic Algorithm in the cylindrical example. (b) Inner and outer imaginary part of the refractive indices using the Bernard Model combined with Genetic Algorithm in the cylindrical example.

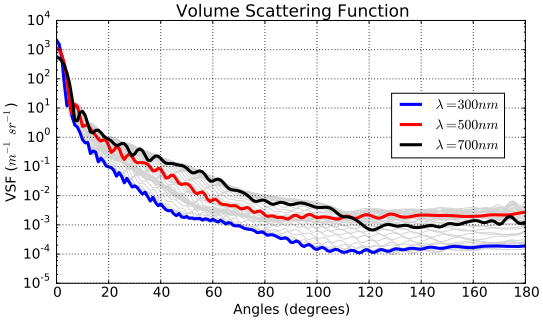

Figure 17. Volume scattering function obtained using the Bernard Model combined with Genetic Algorithm in the cylindrical example.

mogeneous particles with spherical shape are considered instead of the cylinders. This allows using the Lorenz-Mie theory instead the T-matrix approach, dramatically improving the simulation time. Then, the estimated refractive index using homogeneous spheres is finally applied on homogeneous cylinders to obtain their IOP, since the volume scattering function values are case sensitive to the particle shape. Although the slow T-matrix approach is needed for this simulation, it has to be executed only once. For sure, using better computing resources (as for instance, by means of a computer cluster), this problem disappears and the genetic algorithm can be used with its complete potential.

The methodology was applied on this last example using the same PSD of Fig. 12. The estimated complex refractive index is shown in Fig. 18a. The averaged relative error of the real part is 7.75% and 2.61% for the imaginary part. Since absorption is proportional to the volume, the inverted imaginary part of the refractive index agrees well with the assumed values (volume equivalent spheres are being used). However, since scattering depends strongly on the shape of particles, the inverted real part of the refractive index deviates from the assumed values. The major differences are obtained at the lowest wavelengths, which is also noticeable in the volume scattering function, as seen in Fig.

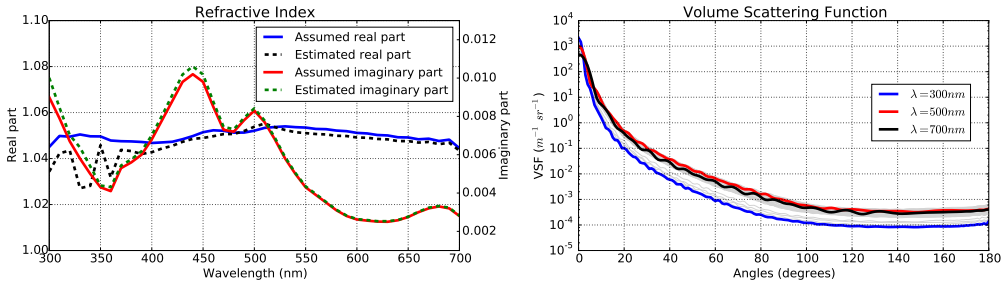

(a) (b)

Figure 18. (a) Assumed and estimated refractive indices using the genetic algorithm for spherical-shaped homogeneous particles, and (b) the volume scattering function.

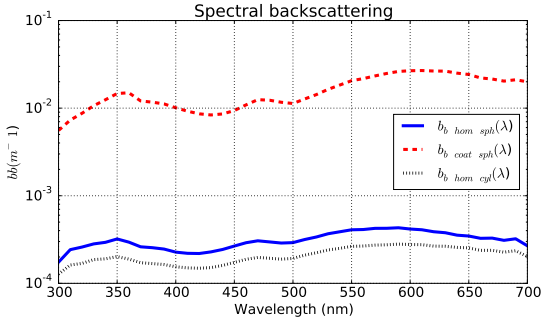

Figure 19. Spectral backscattering of the three test cases: homogeneous sphere, coated sphere and homogeneous cylinder.

18b, with some artefacts in those wavelengths where abrupt changes of the real part of the refractive index occur (330 and 350 nm). However, the averaged relative error committed decreases from 77% in the previous method to 16%. If homogeneous spheres are used instead of cylinders to obtain the IOP, the averaged relative error increases to 22%, which demonstrates that choosing a suitable shape improves the results.

5 Discussion

Table 2 shows the averaged relative errors associated with each method when estimating the real and imaginary parts of the refractive indices and the one committed by the respective volume scattering functions in the three examples of the previous section. In the real part case, the error was obtained using $n-1$ instead of n. Note that the inverse models do not compute the volume scattering function. It is obtained after introducing the estimated complex refractive indices in the suitable forward model, i.e., the Lorenz-Mie or T-Matrix theories.

In the homogeneous sphere example, the Twardowski model presents the highest errors, especially when comparing the volume scattering function. It can also be seen in the table that, although the

Table 2. Averaged relative errors committed in each method

Shapes	**Model**	n **relative error**	k **relative error**	**VSF relative error**
Homogeneous sphere	Twardowski model	42%	44%	68%
	Stramski model	8.2%	15%	0.17%
	Genetic Algorithm	0.004%	0.24%	0.17%
Coated sphere	Genetic Algorithm	-	-	78%
	Bernard model	1.4%	51%	52%
	Bernard model & GA	0.1%	0.14%	0.2%
Homogeneous cylinder	Bernard model & GA	-	-	77%
	Genetic Algorithm[a]	7.75%	2.61%	16% [b]

[a] The refractive index is estimated using spheres but the IOP is obtained using that refractive index in cylinders.
[b] If the cylindrical shape is not used, the error rises up to 22%.

errors of the Stramski model are considerably higher than the ones of the Genetic Algorithm when retrieving the complex refractive index, especially in the imaginary part, similar estimations of the volume scattering function are recovered in both cases. This implies that there is no need of an accurate refractive index estimation in this particular example to obtain a suitable characterization of the scattering properties. However, the Genetic Algorithm performs with an excellent accuracy for the refractive-index retrieval.

In the coated sphere example, the Genetic Algorithm approximates the coated particle to a homogeneous one with a single complex refractive index. Therefore, errors for the inner and outer refractive indices cannot be obtained. Besides, this method presents an important disagreement when computing the volume scattering function. This result shows that, in case the optical behaviour of coated spheres were closer to that of actual phytoplankton particles, as stated in (Bernard et al., 2009), homogeneous spheres would not be a suitable choice to accurately reproduce their optical behaviour. The Bernard model is a fast technique to estimate the inner and outer refractive indices, but mainly fails in estimating the imaginary part of the refractive index (with an error up to 51%). This leads to a significant error committed by the forward model when computing the volume scattering function. However, if the Bernard model is combined with the Genetic Algorithm (the Bernard model is used to estimate the inner refractive index, and the Genetic Algorithm to retrieve the external one), accurate values are obtained for the complex refractive indices and, later, for the volume scattering function in the forward model.

Finally, in the homogeneous cylinder case, it can be seen that the optical properties of this kind of particles are not accurately reproduced using a coated sphere the refractive indices of which are obtained with the combination of the Bernard model and the Genetic Algorithm. From the previous results, it could be expected that the optimal retrieval method would be the Genetic Algorithm using

cylindrical shapes to obtain an accurate estimation. However, this involves using the slow T-Matrix code of Mischenko iteratively, which would require several months to converge (as the particle becomes more aspherical, the convergence time increases considerably). In order to make the retrieval faster, homogeneous spheres with equal volume are used instead of cylinders. The retrieved refractive index is then used to obtain the IOPs using cylinders this time. Using this method, the volume scattering function shows an averaged relative error of 16%, improving the result obtained using spheres (22%). Therefore, this result confirms that selecting a suitable shape is important for an improvement of the modelling (at least in this ideal case).

At this point, three central topics remain to be deeply investigated in order to continue the work presented in this paper:

1. All the test cases presented above are synthetic examples that, presumably, are simpler than real life. Further work must be done in order to study the performance of the algorithms when used with the optical properties of actual phytoplankton species and bulk oceanic measurements. In order to deal with this latter case, where different shapes and refractive indices are mixed in the same sample, a more complex inversion method should be developed. Currently, this problem is approximated using only spherical particles (Boss et al., 2001b, and references therein). However, apart from the particle diameter, the T-Matrix method opens the possibility to consider other parameters associated with the particle shape as well. Thus, a new inversion algorithm based on the T-Matrix and an optimization technique such as the genetic algorithm could be developed to estimate the proportion of each phytoplankton morphological type and their own refractive index. For sure, such algorithm would require an enormous effort in computation, although this is a problem that becomes smaller as technology evolves. Another issue to be examined when dealing with actual phytoplankton is related with the accuracy of the measurement instruments. Attenuation and scattering coefficients are needed as inputs for all of the retrieval methods, and if they are not precise, the retrieved refractive indices will not be as well. As stated by Ramírez-Pérez et al. (2015), the acceptance angle of the optical instruments affect severely on the amplitude of the measurements. By comparing the extinction coefficient of two different instruments with different acceptance angles, different magnitude values were obtained, showing an averaged ratio of 0.67. This is a key issue that must be considered to get reliable results using the presented methodology.

2. The accuracy of the inversion methods can be improved developing new shapes for T-Matrix. For instance, coated cylinders to model algae with a cylindrical shape (as stated by Bernard et al.,2009, in the spherical case, coated particles generate backscattering functions closer to those produced by actual phytoplankton particles) or other outlines more similar to the actual shape of the phytoplankton particles (the T-Matrix approach allows the computation of particle shapes exhibiting axial symmetry, Sun et al.,2016).

3. It is widely known that ocean optics comprises from research on microscopic particles (as shown in this paper) to remote sensing. The inversion methods based on Lorenz-Mie and T-Matrix can be accordingly extended to consider other type of optical measurements in addition to the inherent optical properties, as the remote-sensing reflectance. As an example, Fig. 19 shows the spectral backscattering of the three test cases, the homogeneous sphere, the coated sphere and the homogeneous cylinder. Many operational remote-sensing inversion models for the inherent optical properties use an implicit or explicit assumption about the refractive index. Therefore, if they were combined with the inversion methods presented here, the models could be improved. Retrieving the index of refraction from space would improve the ability to distinguish sources of backscattering from each other in the ocean. To this end, a much more complex inversion scheme should be developed.

To conclude, the results presented in this paper and summarized in Table 2 do not determine which is the best method to estimate the phytoplankton optical properties, since none of them are a realistic representation of real algae where there may be cell walls, chloroplasts, vacuole, nucleus and other internal organelles, each with its own optical properties. However, the assumed particles serve as a first approximation of actual phytoplankton and are useful to extract some preliminary conclusions and to introduce several improvements as an attempt to make the approximations a bit closer to the reality. Most of the methods shown in the paper are already being used for the retrieval of the refractive indices of isolated particles or bulk oceanic distributions, and a comparison of their performance can only be done using well-known models. It has been seen that the Genetic Algorithm is not a fast technique, since several minutes are required for each estimation (when using spherical shapes; slower with aspherical particles) as compared to the few seconds generally required by the other methods, the Twardowski model being the faster of them. However, it is a versatile technique that alone or combined with other methods improve the accuracy of the estimations to a level not achieved by any other method.

6 Conclusions

A performance analysis was carried out in order to examine the accuracy of different inverse methods that use the optical properties of small scatterers and their particle size distribution to retrieve their refractive indices. To this end, three different synthetic examples were constructed, each one with a different shape and distribution. The selected shapes were homogeneous spheres, coated spheres and homogeneous cylinders. Results indicated that those methods using a genetic algorithm to optimize the inversion were the most accurate ones, but also the slowest. In particular, an excellent agreement between estimated and actual refractive indices and volume scattering functions was obtained for the homogeneous and coated sphere cases, and a fair agreement for the homogeneous cylinders. These results suggest that better characterizations could be obtained for the actual phytoplankton optical

properties. Therefore, the next step is a further analysis of the performance of these methods when applied on measurements of isolated cultures of phytoplankton.

Acknowledgements. This work was supported by the Spanish National Research Council (CSIC) under the EU Citclops Project (FP7-ENV-308469), the MESTRAL project (CTM2011-30489-C02-01), and the CSIC ADOICCO project (Ref 201530E063). The authors would also like to show their gratitude to Emmanuel Boss and two anonymous reviewers for their comments and suggestions, which helped to enhance the quality of the manuscript.

References

Aas, E.: Refractive index of phytoplankton derived from its metabolite composition, Journal of Plankton Research, 18, 2223–2249, 1996.

Aden, A. and Kerker, M.: Scattering of electromagnetic waves from two concentric spheres, J. Appl. Phys., 22, 1242–1246, 1951.

Bernard, S., Probyn, T., and Barlow, R.: Measured and modelled optical properties of particulate matter in the southern Benguela, South African Journal of Science, 97, 410–420, 2001.

Bernard, S., Probyn, T., and Quirantes, A.: Simulating the optical properties of phytoplankton cells using a two-layered spherical geometry, Biogeosciences Discuss., 6, 1–67, 2009.

Bhandarkar, S., Zhang, Y., and Potter, W.: An edge detection technique using genetic algorithm-based optimization, Pattern Recognition, 27, 1159 – 1180, 1994.

Bohren, C. and Huffman, D., eds.: Absorption and scattering of light by small particles, New York : Wiley, Oxford, 1998.

Boss, E., Pegau, W., Gardner, W., Zaneveld, J., Barnard, A., Twardowski, M., Chang, G., and Dickey, T.: Spectral particulate attenuation and particle size distribution in the bottom boundary layer of a continental shelf, J. Geophys. Res., 106, 9509–9516, 2001a.

Boss, E., Twardowski, M., and Herring, S.: Shape of the particulate beam attenuation spectrum and its inversion to obtain the shape of the particulate size distribution, Appl. Opt., 40, 4885–4893, 2001b.

Boss, E., Pegau, W., Lee, M., Twardowski, M., Shybanov, E., Korotaev, G., and Baratange, F.: Particulate backscattering ratio at LEO 15 and its use to study particles composition and distribution, J. Geophys. Res., 109, 2004.

Bricaud, A. and Morel, A.: Light attenuation and scattering by phytoplanktonic cells: a theoretical modeling, Appl. Opt., 25, 571–580, 1986.

Bricaud, A., Zaneveld, J., and Kitchen, J.: Backscattering efficiency of coccol-25 ithophorids: use of a three-layered sphere model, In: Ocean Optics XI Proc SPIE, p. 27–33, 1992.

Carder, K., Betzer, P., and Eggimann, D. W., eds.: Physical, chemical, and optical measures of suspended particle concentrations: Their intercomparison and application to the west African shelf, in Suspended Solids in Water, Springer US, Oxford, 1974.

Choi, W., Fang-Yen, C., Badizadegan, K., Oh, S., Lue, N., Dasari, R., and Feld, M.: Tomographic phase microscopy, Nature Methods, 4, 717–719, 2007.

Clavano, W., Boss, E., and Karp-Boss, L.: Inherent optical properties of non-spherical marine-like particles - From theory to observation, Oceanography and Marine Biology: An Annual Review, 45, 1–38, 2007.

Dall'Olmo, G., Westberry, T., Behrenfeld, M., Boss, E., and Slade, W.: Significant contribution of large particles to optical backscattering in the open ocean, Biogeosciences, 6, 947–967, 2009.

Fortin, F., Rainville, F. D., Gardner, M., Parizeau, M., and Gagné, C.: DEAP: Evolutionary algorithms made easy, Machine Learning Research, 13, 2171–2175, 2012.

Gordon, H. and Morel, A.: Remote assessment of ocean color for interpretation of satellite visible imagery: A review, Springer Science and Business Media, 2012.

Greenhalgh, D. and Marshall, S.: Convergence Criteria for Genetic Algorithms, J. on Computing, 30, 269–282, 2000.

Hahn, S. L.: Hilbert transforms in signal processing, Artech House on Demand, 1996.

Hale, G. and Querry, M.: Optical constants of water in the 200-nm to 200-μm wavelength region, Appl. Opt., 12, 555–563, 1973.

Hold-Geoffroy, Y., Gagnon, O., and Parizeau, M.: Once you SCOOP, no need to fork, in: Proceedings of the 2014 Annual Conference on Extreme Science and Engineering Discovery Environment, p. 60, ACM, 2014.

Kirk, J. T.: Light and photosynthesis in aquatic ecosystems, Cambridge University Press, 1994.

Latimer, P.: Light scattering by a homogeneous sphere with radial projections, Appl. Opt., 23, 442–447, 1984.

Lorenz, L.: Sur la lumière réfléchie et réfractée par une sphère (surface) transparente, vol. I of *Oeuvres scientifiques de L. Lorenz. Revues et annotées par H. Valentiner*, Librairie Lehmann et stage, Copenhagen, 1898.

Mera, N., Elliott, L., and Ingham, D. B.: A multi-population genetic algorithm approach for solving ill-posed problems, Computational Mechanics, 33, 254–262, 2004.

Meyer, R.: Light-scattering from biological cells - Dependence of backscatter radiation on membrane thickness and refractive index, Appl. Optics, 18, 585–588, 1979.

Mie, G.: Beiträge zur Optik trüber Medien, speziell kolloidaler Metallösungen, Annalen der Physik, 330, 377–445, 1908.

Mischenko, M. and Travis, L.: Capabilities and limitations of a current Fortran implementation of the T-matrix method for randomly oriented, rotationally symmetric scatterers, Quant. Spectrosc. Radiat. Transfer, 60, 309–324, 1998.

Mischenko, M., Travis, L., and Mackowski, D.: T-matrix computations of light scattering by nonspherical particles: a review, Quant. Spectrosc. Radiat. Transfer, 55, 535–575, 1996.

Mobley, C., ed.: Light and Water: Radiative Transfer in Natural Waters, Academic Press, 1994.

Morel, A.: Diffusion de la lumière par les eaux de mer; résultats expérimentaux et approche théorique, Optics of the Sea, AGARD Lecture Ser., 61, 3.1.1.–3.1.76, 1973.

Mugnai, A. and Wiscombe, W.: Scattering from nonspherical Chebyshev particles. I: cross sections, single-scattering albedo, asymmetry factor, and backscattered fraction, Appl. Opt., 25, 1235–1244, 1986.

Nocedal, J. and Wright, S., eds.: Numerical Optimization, New York : Springer, 1999.

Quirantes, A.: A T-matrix method and computer code for randomly oriented, axially symmetric coated scatterers, Quant. Spectrosc. Radiat. Transfer, 92, 373–381, 2005.

Quirantes, A. and Bernard, S.: Light scattering by marine algae: two-layer spherical and nonspherical models, Quant. Spectrosc. Radiat. Transfer, 89, 311–321, 2004.

Quirantes, A. and Bernard, S.: Light-scattering methods for modelling algal particles as a collection of coated and/or nonspherical scatterers, Quant. Spectrosc. Ra., 100, 315–324, 2006.

Ramírez-Pérez, M., Röttgers, R., Torrecilla, E., and Piera, J.: Cost-effective hyperspectral transmissometers for oceanographic applications: performance analysis, Sensors, 15, 20 967–20 989, 2015.

Sánchez, A., Zafra, E., and Piera, J.: Hyperspectral characterization of marine particles based on Mie-Lorentz and T-matrix codes and a genetic algorithm, in: Workshop on Hyperspectral Image and Signal Processing: Evolution in Remote Sensing (WHISPERS), IEEE, 2014.

Stramski, D., Morel, A., and Bricaud, A.: Modeling the light attenuation and scattering by spherical phytoplanktonic cells: a retrieval of the bulk refractive index, Appl. Opt., 27, 3954–3956, 1988.

Stramski, D., Bricaud, A., and Morel, A.: Modeling the inherent optical properties of the ocean based on the detailed composition of the planktonic community, Appl. Opt., 40, 2929–2945, 2001.

Stramski, D., Boss, E., Bogucki, D., and Voss, K.: The role of seawater constituents in light backscattering in the ocean, Progress in Oceanography, 61, 27–56, 2004.

Sun, B., Kattawar, G., Yang, P., Twardowskic, M., and Sullivan, J.: Simulation of the scattering properties of a chain-forming triangular prism oceanic diatom, Quant Spectrosc Radiat Transfer, Available online, 2016.

Twardowski, M., Boss, E., Macdonald, J., Pegau, W., Barnard, A., and Zaneveld, J.: A model for estimating bulk refractive index from the optical backscattering ratio and the implications for understanding particle composition in case I and case II waters, Geophysical Research: Oceans, 106, 14 129–14 142, 2001.

van de Hulst, H., ed.: Ligh scattering by small particles, New York : Wiley, Oxford, 1957.

Volz, F.: Die optik und meteorologie der atmosphärishen trubung, Ber. Dtsch. Wetterdienstes, 13, 1–47, 1954.

Waterman, P.: Matrix formulation of electromagnetic scattering, Proceedings of the IEEE, 53, 805–812, 1965.

Wiscombe, W. and Grams, G.: The backscatered fraction in two-stream approximations, Journal of the Atmospheric Sciences, 33, 2440–2451, 1976.

Zaneveld, J. and Kitchen, J.: The variation in the inherent optical properties of phytoplankton near an absorption peak as determined by various models of cell structure, Geophys. Res., 100(C7), 13 309–13 320, 1995.

Zhu, C., Byrd, R., and Nocedal, J.: L-BFGS-B: Algorithm 778: L-BFGS-B, FORTRAN routines for large scale bound constrained optimization, ACM Transactions on Mathematical Software, 23, 550–560, 1997.